Synthesis and experimental investigation of PZT nanocomposite films

IOP Conf. Series: Materials Science and Engineering **715** (2020) 012058 doi:10.1088/1757-899X/715/1/012058

Synthesis and experimental investigation of PZT nanocomposite films

Tomas Janusas, Giedrius Janusas*, Arvydas Palevicius and Justas Ciganas

Kaunas University of Technology, Faculty of Mechanical Engineering and Design, Studentu 56, 51424 Kaunas, Lithuania

*Email: giedrius.janusas@ktu.lt

Abstract. In this paper, synthesis of nanocomposite and experimental investigation of three samples of nanocomposite films are presented. The aim of this research is to determine influence of the PZT particle concentration in nanocomposite on the surface morphology, qualitative and quantitative chemical composition ant direct piezoelectric effect. The specimens were prepared by mixing the PZT nanopowder with PMMA in three different proportions: 85% of PZT and 15% of binder; 90% of PZT and 10% of binder; 95% of PZT and 5% of binder. Surface morphology and qualitative and quantitative chemical composition were evaluated using scanning electron microscope, which is equipped with the Energy Dispersive X-Ray Spectrometer. Electrical response of the pulse-excited specimens is also presented.

1. Introduction

Creation of the effective micromechanical fluidic systems increases efficiency of microdosing or fluid microflow control, resulting reduced analysis time of the biological fluids and increased applicability in biosensors. Active microfluidic components [1, 2] and platforms [3, 4] have been developed. However, some disadvantages are still unsolved. Ability to manipulate microvolume fluids or increase the flow speed is the key in the development of single particle biosensors [5]. Techniques of microfluid flow control using standing or traveling surface acoustic waves [6] or bulk acoustic waves [7] are very well known. These techniques are based on generation of acoustic waves in micromechanical fluidic devices using piezoelectric, electromagnetic and other active materials.

Thin layer PZT films have been used for a long time in MEMS systems [8], but only in 2018 P. Reichert et. al. [9] proposed to apply them in microfluidic devices to generate bulk acoustic waves, which enable controlling the bio particles effectively using low voltage and making minimal effect on temperature of analysed analyte. The quality factor of these micromechanical fluidic elements depends on the piezoelectric materials, that are used for formation of microfluidic devices. Researchers S. Siddiqui [10], K. Choi [11], H. Parangusan [12], S. Osho [13], J. Belovickis [14], and others, from all over the world are working on the development of piezoelectric composites. Efficiency, quality and application of the piezoelectric nanocomposites are the main areas of the research in this topic.

This research paper covers the investigation of piezoelectric nanocomposite material employed as microresonators, which could ensure more effective flow of microfluids when the system is excited by vibrations. The impact of different PZT nanoparticles concentration on the PZT nanocomoposite film

properties was analysed. Thus, three unique specimens made of PZT nanocomposite material were fabricated and tested.

2. Materials and experimental setup

2.1. PZT nanocomposite synthesis

The fabrication of the PZT nanocomposite material starts with powder preparation. This composite material was designed by mixing PZT nanopowder with poly methyl methacrylate (PMMA) in three different proportions: 85% of PZT and 15% of binder (PZT85); 90% of PZT and 10% of binder (PZT90); 95% of PZT and 5% of binder (PZT95).

An oxalate/hydroxide co-precipitation method was used for synthesis of lead zirconate titanate [Pb $(Zr_{0.52}Ti_{0.48})O_3$] nanopowder. The materials used were lead (II) acetate $Pb(CH_3COO)_2$, titanium butoxide $Ti(C_4H_9O)_4$, zirconium butoxide $Zr(C_4H_9O)_4$ (80 % solution in n-butanol), oxalic acid dihydrate $C_2H_2O_4 \bullet 2H_2O$, 25% ammonia solution and deionized water. The detailed description of synthesis is presented in paper [15].

Layer (60 μm thickness) of PZT nanocomposite materials (PZT85, PZT90, PZT95) was formed on the copper foil using screen printing technique with the polyester monofilament screen mesh (48/70) and dried in electrical oven at 100 °C for 30 min (figure 1).

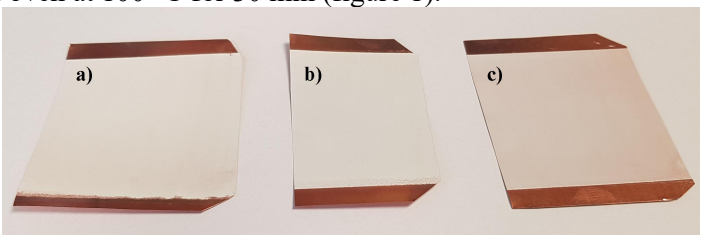

Figure 1. Prepared samples: a) PZT85, b) PZT90, c) PZT95.

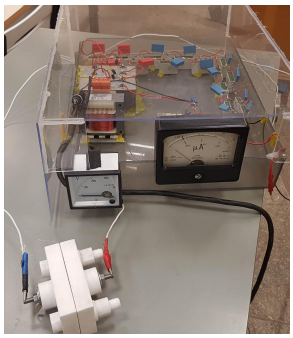

Figure 2. High voltage set for the pole alignment of PZT coatings.

In order to improve piezoelectric characteristics of the formed PZT nanocomposite with PMMA binder electrical pole alignment was performed using a high voltage generator and a custom–made holder, shown in figure 2. An element with a PZT coating was placed in the special holder between positive and negative poles. The high voltage generator was set at 5 kV current and held for 30 min. The poling technique aligns a positive pole on one side of the PZT coating and a negative pole on the other side. Prepared specimens were tested and compared with the results presented in papers [15, 16].

2.2. Surface morphology and chemical composition

Surface morphology and chemical composition of the formed PZT nanocomposite materials were evaluated using scanning electron microscope (SEM) FEI Quanta 200 FEG, equipped with the Energy Dispersive X-Ray Spectrometer (EDS) detector XFlash 4030 from Bruker. Samples were investigated under controlled pressure water steam atmosphere. Maximal achievable resolution for high-vacuum (< 6e-4 Pa) is 1.2 nm, for low-vacuum (10 to 130 Pa) – 2.5 nm and for extended vacuum mode (10 to 4000 Pa) – 3 nm. The EDS detector allows detecting elements ranging from boron (5) to americium

(95). The chemical analysis can be determined at the chosen point, along the line or distribution on the surface – mapping also is a possibility. A modern 30 mm^2 area solid state drift detector is cooled with Peltier element and provides 133 eV (at Mn K) energy resolution at 100,000 cps. Moreover, X-Ray spectroscopy method allows analysing energy distributions, i.e. the energy differences between the various quantum states of a system and the probabilities that the system jumps between these states.

2.3. Dynamic and electric characterisation

The dynamic and electric characteristics of the multilayer specimens were investigated using the laser triangular displacement sensor: sensitive head LK-G82 and control unit LK–GD500. The measured vibration amplitude was collected with a USB oscilloscope PicoScope 3424. The experimental setup is presented in figure 3. It was used to investigate the electrical response of the multilayer specimens upon calibrated mechanical pulse of 10 N.

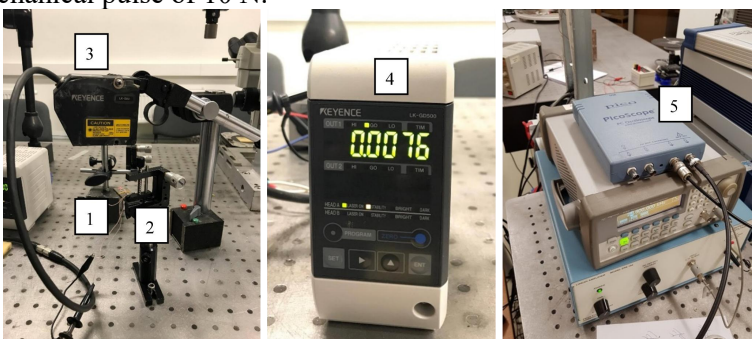

Figure 3. Experimental setup for dynamic and electric characterization of specimens: 1 – specimen; 2 – holder; 3 – sensor head LK-G82; 4 – control block LK-G500; 5 – USB oscilloscope PicoScope 3424.

3. Results

In this research, three samples of nanocomposite films were fabricated and investigated. The SEM views and EDS spectrums of PZT85, PZT90 and PZT95 nanocomposite films on Cu substrate are presented in figure 4 – figure 6.

The surface morphology of the first sample PZT85 (figure 3a) shows non even distribution of PZT particles of the size up to 1 μm. Also small pileups of 5 – 10 μm in diameter were observed on top of the surface. The SEM view of the nanocomposite PZT90 showed better distribution of PZT particles (figure 5a). Whereas, the surface view of the nanocomposite PZT95 showed even distribution of PZT particles. Finally, the results showed that a PMMA binder loaded with bigger amount of the PZT particles ensures the higher surface quality, thus forming a much more promising sensing and actuating. Simultaneously, formation of active microfluidic devices using thermal formation process [17] could be too complicated.

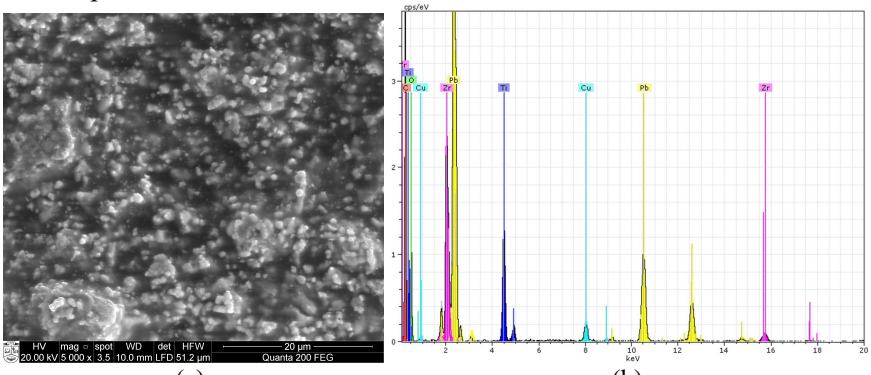

(a) (b)

Figure 4. Surface morphology (a) and energy dispersive spectrum (b) of the piezoelectric nanocomposite PZT85.

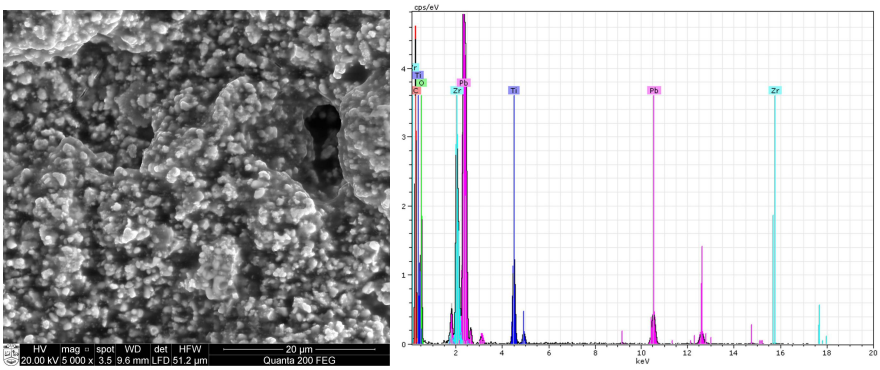

(a) (b)

Figure 5. Surface morphology (a) and energy dispersive spectrum (b) of the piezoelectric nanocomposite PZT90.

EDS analysis gives qualitative and quantitative determinations of the elemental composition of the piezoelectric nanocomposites. These microanalyses show the dominance of lead, with a Lα peak at 10.6 keV, Lβ peak at 12.6 keV and Mα peak at 2.3 keV, and oxygen with a Kα peak at 0.5 keV (Figure 4.b – Figure 6.b). Other peaks show the smaller quantities of carbon (Lα peak at 0.3 keV), zirconium (Kα peak at 15.8 keV, Kβ peak at 17.7 keV, Lα peak at 2 keV and Lβ peak at 2.1 keV) and titanium (Kα peak at 4.5 keV, Kβ peak at 4.9 keV, Lα peak at 0.4 keV and Lβ peak at 0.5 keV). In addition, minor amount of copper with a Kα peak at 8 keV, Kβ peak at 8.9 keV, Lα peak at 0.93 keV and Lβ peak at 0.95 keV was detected in the specimen of PZT85. The detailed information of the normalized concentration in weight percent of the chemical composition of the piezoelectric nanocomposites PZT85, PZT90 and PZT95 is presented in table 1.

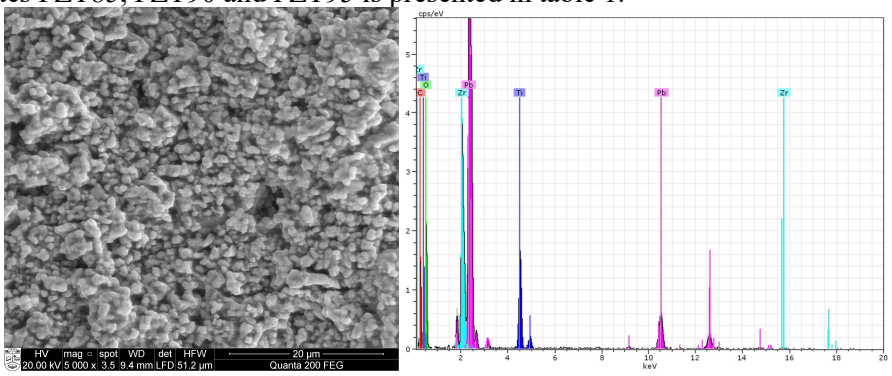

(a) (b)

Figure 6. Surface morphology (a) and energy dispersive spectrum (b) of the piezoelectric nanocomposite PZT95.

Table 1. Chemical composition of the piezoelectric nanocomposites PZT85, PZT90 and PZT95.

Chemical elements	The normalized concentration in weight percent (norm. wt., %)		
	PZT85	PZT90	PZT95
Carbon	17.6	24.9	11.8
Oxygen	55.3	31.2	28.5
Titanium	3.6	5.2	7.1
Copper	0.9	0	0
Zirconium	5.4	12.2	13.4
Lead	17.2	26.5	39.2

Direct piezoelectric effect of the three fabricated PZT nanocomposites was investigated using experimental setup described in Section 2.3. All specimens were pulse-excited using calibrated

mechanical pulse of 10N. Open circuit voltage generated by all three specimens was measured and collected using USB oscilloscope PicoScope 3424 (figure 7). The specimen coated by PZT95 nanocomposite film showed the best results. It generated electrical pulse of 0.36 mV. Specimen with PZT90 film generated voltage of 0.08 V and specimen with PZT90 film generated 0.2 V electrical pulse. In comparison with previously achieved results [11] generated voltage increases. However, application area of this piezoelectric nanocomposite became more complicated due to its bigger microhardness.

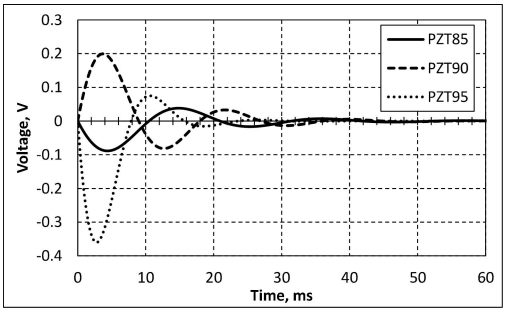

Figure 7. Generated voltage by pulse-excited PZT nanocomposite films.

4. Conclusion

In this research, three samples of nanocomposite films were fabricated and investigated. PZT nanopowder was mixed with PMMA in three different proportions: 85% of PZT and 15% of binder; 90% of PZT and 10% of binder; 95% of PZT and 5% of binder. The SEM views showed that higher PZT concentration leads to better surface quality and even distribution of PZT nanoparticles. The microanalyses using EDS spectrums showed the dominance of lead and oxygen in the PZT nanocomposite. Other peaks showed smaller quantities of carbon, zirconium and titanium. Quantities of all chemical components vary and correlate with the concentration of PZT nanoparticles. The better surface quality of specimen PZT95 was confirmed by the measurement of the direct piezoelectric effect of PZT nanocomposites using pulse-excitation. It showed that PZT nanocomposite of the higher PZT particle concentration generates up to 4 times higher electrical potential. The change in chemical composition of the PZT nanocomposite helps to manipulate the mechanical and piezoelectric characteristics for different applications.

Acknowledgments

This research was funded by a grant S-MIP-17-102 from the Research Council of Lithuania.

References

[1] C.I. Rogers, J.B. Oxborrow, R.R. Anderson, L.F. Tsai, A.T. Woolley, Sens. Actuators B Chem. **191** (2014).
[2] J. Thomas, Z. Tehrani, B. Redfearn, Addit. Manuf. **9** (2016).
[3] R. Burger, L. Amato, A. Boisen, Biosens. Bioelectron. **76** (2016).
[4] X. Wang, D. Nilsson, P. Norberg, Biochim. Biophy. Acta (BBA) Gen. Subj. **1830** (2013).
[5] J.J. Gooding, K. Gaus, Angewandte Chemie International Edition **55**, 38 (2016).
[6] A. Mujahid, F.L. Dickert, Sensors **17**, 12 (2017).
[7] Y. Chang, Z. Hui, X. Wang, H. Qu, W. Pang, X. Duan, Sensors **18**, 2 (2018).
[8] S.T. Mc Kinstry, P. Muralt, Journal of Electroceramics **12**, 1–2 (2004).
[9] P. Reichert, D. Deshmukh, L. Lebovitz, J. Dual, Lab on Chip (2018).
[10] S. Siddiqui, D.I. Kim, L.T. Duy, M.T. Nguyen, S. Muhammad, W.S. Yoon, N.E. Lee, Nano Energy **15** (2015).
[11] K. Choi, W. Choi, C. Yu, Y.T. Park, Journal of Nanomaterials (2017).
[12] H. Parangusana, D. Ponnamma, M. Al Ali Al Maadeed, RSC Adv. **7** (2017).
[13] S. Osho, N. Wu, M. Aramfard, C. Deng, O. Ojo, Smart Mater. Struct. **27** (2018).

[14] J. Belovickis, M. Ivanov, V. Samulionis, J. Banys, A. Solnyshkin, S.A. Gavrilov, K.N. Nekludov, V.V. Shvartsman, M.V. Silibin, Physica status solidi (b) **255**, 3 (2018).
[15] E. Cekas, G. Janusas, A. Guobiene, A. Palevicius, A. Vilkauskas, S. Ponelyte-Urbaite, Sensors **18**, 11 (2018).
[16] G. Janusas, S. Ponelyte, A. Brunius, A. Guobiene, A. Vilkauskas, A. Palevicius, Sensors **16**, 11 (2016).
[17] A. Sodah, R. Gaidys, B. Narijauskaite, R. Sakalys, G. Janusas, A. Palevicius, P. Palevicius. Microsystem technologies (2018).